New Phytologist

Seedling developmental defects upon blocking CINNAMATE-4-HYDROXYLASE are caused by perturbations in auxin transport'

Journal:	*New Phytologist*
Manuscript ID	NPH-MS-2021-35525.R1
Manuscript Type:	MS - Regular Manuscript
Date Submitted by the Author:	n/a
Complete List of Authors:	El Houari, Ilias ; Ghent University, Department of Plant Biotechnology and Bioinformatics; VIB, Center for Plant Systems Biology Van Beirs, Caroline; Ghent University, Department of Plant Biotechnology and Bioinformatics; VIB, Center for Plant Systems Biology Arents, Helena; Ghent University, Department of Plant Biotechnology and Bioinformatics; VIB, Center for Plant Systems Biology Han, Huibin; Institute of Science and Technology Austria, IST Chanoca, Alexandra; Ghent University, Department of Plant Biotechnology and Bioinformatics; VIB, Center for Plant Systems Biology Opdenacker, Davy; Ghent University, Department of Plant Biotechnology and Bioinformatics; VIB, Center for Plant Systems Biology Pollier, Jacob; Ghent University, Department of Plant Biotechnology and Bioinformatics; VIB, Center for Plant Systems Biology; VIB, Metabolomics Core Facility Storme, Véronique; Ghent University, Department of Plant Biotechnology and Bioinformatics; VIB, Center for Plant Systems Biology Steenackers, Ward; Ghent University, Department of Plant Biotechnology and Bioinformatics; VIB, Center for Plant Systems Biology Quareshy, Mussa; University of Warwick, School of Life Sciences Napier, Richard; The University of Warwick, School of Life Sciences Beeckman, Tom; Ghent University, Department of Plant Biotechnology and Bioinformatics; VIB, Center for Plant Systems Biology Friml, Jiri; IST Austria, Department of Plant Systems Biology De Rybel, Bert; Ghent University, Department of Plant Biotechnology and Bioinformatics; VIB, Center for Plant Systems Biology Boerjan, Wout; Ghent University, Department of Plant Biotechnology and Bioinformatics; VIB, Center for Plant Systems Biology Vanholme, Bartel; Ghent University, Plant Systems Biology
Key Words:	phenylpropanoids, lignin, auxin, cis-cinnamic acid, Arabidopsis, piperonylic acid, roots, metabolomics

Seedling developmental defects upon blocking CINNAMATE-4-HYDROXYLASE are caused by perturbations in auxin transport

Ilias El Houari[a,b], Caroline Van Beirs[a,b], Helena E. Arents[a,b], Huibin Han[c], Alexandra Chanoca[a,b], Davy Opdenacker[a,b], Jacob Pollier[a,b,d], Véronique Storme[a,b], Ward Steenackers[a,b], Mussa Quareshy[e], Richard Napier[e], Tom Beeckman[a,b], Jiří Friml[c], Bert De Rybel[a,b], Wout Boerjan*[a,b], Bartel Vanholme*[a,b]

* these authors share last authorship.

[a]Ghent University, Department of Plant Biotechnology and Bioinformatics, Technologiepark 71, B-9052 Ghent, Belgium [b]VIB Center for Plant Systems Biology, Technologiepark 71, B-9052 Ghent, Belgium [c]Institute of Science and Technology (IST) Austria, 3400 Klosterneuburg, Austria [d]VIB Metabolomics Core, 9052 Ghent, Belgium [e]School of Life Sciences, University of Warwick, Coventry, CV4 7AL, United Kingdom

Corresponding authors: Bartel Vanholme, Wout Boerjan

Email: Bartel.Vanholme@psb.vib-ugent.be; Wout.Boerjan@psb.vib-ugent.be

Phone: +32 9 331 38 40; +32 9 331 38 81

Total word count: **6564**

Introduction word count: **806** Material and methods word count: **1010**

Results word count: **3659** Discussion word count: **1089**

Number of figures: **7** Number of tables: **1**

Supporting information**: Methods S1- S4**

SUMMARY

• The phenylpropanoid pathway serves a central role in plant metabolism, providing numerous compounds involved in diverse physiological processes. Most carbon entering the pathway is incorporated into lignin. Although several phenylpropanoid pathway mutants show seedling growth arrest, the role for lignin in seedling growth and development is unexplored.

• We use complementary pharmacological and genetic approaches to block CINNAMATE-4-HYDROXYLASE (C4H) functionality in Arabidopsis seedlings and a set of molecular and biochemical techniques to investigate the underlying phenotypes.

• Blocking C4H resulted in reduced lateral rooting and increased adventitious rooting apically in the hypocotyl. These phenotypes coincided with an inhibition in auxin transport. The upstream accumulation in *cis*-cinnamic acid was found to likely cause polar auxin transport inhibition. Conversely a downstream depletion in lignin perturbed phloem-mediated auxin transport. Restoring lignin deposition effectively reestablished phloem transport and, accordingly, auxin homeostasis.

• Our results show that the accumulation of bioactive intermediates and depletion in lignin jointly cause the aberrant phenotypes upon blocking C4H, and demonstrate that proper deposition of lignin is essential for the establishment of auxin distribution in seedlings. Our data position the phenylpropanoid pathway and lignin in a new physiological framework, consolidating their importance in plant growth and development.

Keywords: Phenylpropanoids, lignin, auxin, cis-cinnamic acid, Arabidopsis, piperonylic acid, roots, metabolomics

MAIN TEXT

INTRODUCTION

The phenylpropanoid pathway (PPP) is a plant-specific metabolic pathway converting the aromatic amino acids phenylalanine or tyrosine into a broad range of secondary metabolites, including coumarins, phenolic acids, stilbenes and flavonoids (Vogt, 2010). These molecules are involved in a diverse set of biological and physiological processes in plants, ranging from pigmentation to plant defense responses (Saslowsky et al., 2000; Noel et al., 2005; Chong et al., 2009; Schmid et al., 2014; Brunetti et al., 2018; Vanholme et al., 2019c). In quantitative terms, the majority of the carbon entering the PPP is allocated to the biosynthesis of monolignols such as coniferyl and sinapyl alcohol (Boerjan et al., 2003; Vanholme et al., 2019b). The monolignols are the main building blocks of lignin (Boerjan et al., 2003; Ralph et al., 2019; Vanholme et al., 2019b), a biopolymer deposited in the plant cell wall to safeguard the plant's structural integrity as well as long-distance water transport.

Mutations in the PPP often come with dwarfism, and three different models have been proposed that explain these phenotypes (Muro-Villanueva et al., 2019). Two models suggest a change in lignin content and composition to be the causal factor. According to the first model, lignin depletion in xylem vessels causes a weakening in the strength of these cells. The tension forces generated by transpiration then cause the collapse of weakened xylem vessels, thus disrupting xylem functionality (Franke et al., 2002; Coleman et al., 2008; De Meester et al., 2018; Muro-Villanueva et al., 2019). As such, the upward transport of water in the plant is disrupted. The second model proposes a cell wall integrity system to induce dwarfism. The depletion in lignin content or alteration of lignin composition in the cell wall can lead to the induction of a defense response in the plant, which would then negatively impact growth (Gallego-Giraldo et al., 2018). The mediator complex was found to play a central role in the growth inhibition underlying disruption of cell wall integrity (Bonawitz et al., 2014; Dolan et al., 2017). In contrast to the previous two, the third model explaining dwarfism in PPP mutants proposes a differential accumulation of bioactive intermediates to be at the basis of the growth phenotypes.

Several intermediates or end-products of the PPP have been described to have bioactive properties (Vanholme et al., 2019a). Some of the best-described include flavonoids (Peer and Murphy, 2007), salicylic acid (Zhao et al., 2015; Tan et al., 2020) and *cis*-cinnamic acid (Steenackers et al., 2017; Steenackers et al., 2019), but preliminary evidence exists for many more. For some PPP mutants the phenotypes have previously been linked to accumulating flavonoids and salicylic acid (Besseau et al., 2007; Gallego-Giraldo et al., 2011), although for flavonoids this has been disputed (Li et al., 2010).

The phenotypically most severe Arabidopsis PPP mutants are defective in single copy genes, such as *HCT*, *CINNAMATE-4-HYDROXYLASE* (*C4H*) and *COUMARATE-3-HYDROXYLASE* (*C3H*) (Hoffmann et al., 2004; Abdulrazzak et al., 2006; Besseau et al., 2007; Schilmiller et al., 2009; Gallego-Giraldo et al., 2011). A previously described *c4h* T-DNA mutant showed seedling lethality and early arrest of leaf expansion (Schilmiller et al., 2009). In contrast, whereas knockdown mutants showing leaky expression of *C4H* also show a strongly decreased lignin content (*ref3-1*, *ref3-2* and *ref3-3*), they were able to develop into adult plants (Schilmiller et al., 2009). This indicates that a complete block of the pathway is necessary to bring about seedling growth arrest. The underlying cause for the seedling-stage growth phenotypes upon blocking lignin production was however never investigated. This makes the role for lignin in such an early stage of plant development still enigmatic, leaving open possible unexplored functionalities.

Here, we investigated the early developmental defects caused by loss-of-function of C4H, which is the second enzyme active in the PPP, converting *trans*-cinnamic acid (*t*-CA) to *p*-coumaric acid (*p*CA) (Fig. **1a**). Both *c4h* mutant seedlings (*c4h-4*) and seedlings treated with the C4H inhibitor piperonylic acid (PA) (Schalk et al., 1998) showed a perturbed lateral rooting and an accumulation of adventitious roots specifically in the apical region of etiolated hypocotyls. We showed that these phenotypes can be attributed to a perturbation in auxin transport, likely caused by both the accumulation of the auxin transport inhibitor *cis*-cinnamic acid (*c*-CA) and a depletion of lignin. Our results thus show that two proposed models explaining growth perturbation in PPP mutants can underlie the same phenotype within one mutant. In addition, the depletion in lignin caused a perturbation in phloem-mediated auxin transport, presumably due to a disrupted xylem functionality. The restoration of lignin deposition in the *c4h-4* mutant and in PA-treated

seedlings effectively restored both transport streams, resulting in a restoration of auxin distribution over the seedling. Our findings thus propose lignin deposition not only to be essential in providing mechanical strength to support large plant structures, but also as necessary for allowing the correct organization of seedling growth and architecture.

MATERIALS AND METHODS

Plant Material, Transgenic Lines, Chemicals, and Growth Conditions

Arabidopsis thaliana of the Col-0 ecotype was used for all assays unless stated otherwise. The following transgenic lines in the Col-0 ecotype were used: *coi1-21* (Kim et al., 2013), *etr1-3* (Zipfel et al., 2004), *tir1afb2afb3* (Dharmasiri et al., 2005), *pDR5::LUC* (Moreno-Risueno et al., 2010), *tt4* (Brown et al., 2001). The *c4h-4* mutant (GK-753B06; (Kleinboelting et al., 2012)) was obtained from the NASC institute. Seeds were vapor-phase sterilized and grown on ½ Murashige and Skoog (MS) medium (pH 5.7) containing 2.15 g MS basal salt mixture powder (Duchefa), 10 g sucrose, 0.5 g MES monohydrate, 8 g plant tissue culture agar per liter. The medium was supplemented with one of the following compounds: piperonylic acid (PA; Sigma Aldrich), naphthylphthalamic acid (NPA; Sigma Aldrich), coniferaldehyde (ConAld; Sigma Aldrich), salicylic acid (Sigma Aldrich), *p*-coumaric acid (*p*CA; Sigma Aldrich) and quercetin (Sigma Aldrich). These compounds were prepared as a stock solution in DMSO and were added to the autoclaved medium prior to pouring the plates. Seeds were stratified via a two-day cold treatment. For primary root analysis, the plates were incubated for a 14-day-period in a vertical orientation in the tissue culture (TC) room under a 16-h-light/8-h-dark photoperiod at 21°C. For the AR assays, seeds were given a light pulse and then transferred for 7 days to darkness at 21°C. Subsequently the plates were transferred to the TC room for 7 days. For assessment of the involvement of *cis*-cinnamic acid, plants were grown in both the TC room and in a climate-controlled box containing LED lighting.

Phenotyping

Primary root characteristics were assessed by counting the lateral roots along the primary root using a stereomicroscope (CETI Binocular Zoom Stereo). The plates were scanned

using an Epson Expression 11000XL, and root length was measured using the ImageJ software. LRD was calculated by dividing the number of lateral roots for each plant by the respective primary root length. For assessment of adventitious root characteristics, the number of adventitious roots was counted separately for the top third and lower two-thirds along the hypocotyl using a stereomicroscope. The plates were scanned using an Epson Expression 11000XL, and hypocotyl length was measured using the ImageJ software.

pDR5::LUC assays

Plates containing ½ MS medium were sprayed with 1 mM D-luciferin solution (Duchefa Biochemie) and seedlings were subsequently transferred to these plates. The *pDR5::LUC* images were taken by a Lumazone machine carrying a CCD camera (Princeton Instruments). The CCD camera that is controlled by a WinView/32 software imaged the LUC expression automatically every 10 min (exposure time, 10 min) for 12 h. The picture series were saved as TIFF format for further analysis and a Kymograph (http://www.embl.de/eamnet/html/body_kymograph.html) was generated with ImageJ. For quantification of the LUC signal, pixel intensity was measured using ImageJ over the hypocotyl after 1h of imaging. For each seedling, the signal intensity was normalized for the length of the hypocotyl.

Auxin transport assays

Col-0 seeds were sown *in vitro* on ½ MS medium plates contain 50 µM of PA or the same amount of DMSO for 4 days in the darkness, upon which the etiolated seedlings were transferred to the respective light conditions for another 2 days. A positive control was performed using 10 µM NPA. A droplet of 5 µl of ^{3}H-IAA (20 µL of ^{3}H-IAA was added into 10 mL of ½ MS medium with 1.25% agar) was applied to the apical part of the hypocotyls. After an incubation in darkness for 6 hours, the roots were removed and hypocotyls were collected. Samples were homogenized in liquid nitrogen and incubated with 1 mL of Opti-Fluor scintillation cocktail (Perkin Elmer) overnight. Amount of transported ^{3}H-IAA was

then measured in a scintillation counter (Hidex 300SL) for 300 s with three technical repetitions.

Vascular conductivity assays

Seedlings were given a 7-day dark treatment and given a 5-day light treatment. For phloem transport assays, one of the cotyledons of the etiolated seedlings was slightly damaged. The seedling was then placed on a plate containing ½ MS medium with the top part of the hypocotyl being placed on parafilm, and a 1 µL droplet of a 2 mM solution of 5(6)-carboxyfluorescein diacetate (CFDA; Sigma-Aldrich) was applied to the cotyledon. The seedlings were then scored for the presence of signal in the root-hypocotyl junction over a period of 90 min with a 10-min time interval. For xylem transport assays the hypocotyls of etiolated seedlings were excised via a cut slightly above the root-hypocotyl junction. The hypocotyl was placed on a plate containing ½ MS medium with the bottom part of the hypocotyl being placed on parafilm. A 2 µL droplet of a 2 mM solution of CFDA was applied to the bottom part of the hypocotyl. The seedlings were then scored for the presence of signal in the SAM over a period of 30 minutes with a 5-minute time interval.

Wiesner staining

Whole etiolated seedlings were placed in cold aceton for 30 minutes. Seedlings were then placed in Wiesner reagent (3% phloroglucinol, 2 volumes 100% EtOH, 1 volume 37% HCl) for 5 minutes and mounted on slides containing chloral hydrate. Whole-seedling imaging was performed using a Keyence VHX-5000 microscope. Detailed images of the vascular tissue were taken using an Olympus BX53 microscope.

Vascular anatomy

Plant material was fixated in 4% (m/v) paraformaldehyde, 1% (v/v) glutaraldehyde and 0.02 M sodium phosphate buffer (pH 7.2). The material was washed and dehydrated by subsequent incubation steps of 2 hours in ethanol (EtOH) solutions with increasing concentrations (30%, 50%, 70%, 85%, 95%). Infiltration was performed according to

Technovit 7100 (Heraeus Kulzer, Germany) manufacturer instructions. The two-step embedding was performed as described previously (De Smet et al., 2004). Sections of 10 µm were cut using a microtome (Supercut 2050, Reichert-Jung, Germany) and were placed on Superfrost® slides (Menzel Gläser). The staining was done with 0.1% Toluidine Blue O (Sigma) for 10 min, and counterstaining with ruthenium red (Sigma), with washing steps between and after staining. DePeX Mounting Medium (VWR) treatment was performed and pictures were taking using a DIC light microscope (Leica BX51) with an industrial digital camera using ToupView 3.7 software.

RESULTS

1. Blocking the phenylpropanoid pathway affects seedling development

To study the early growth phenotypes of *c4h* knockout plants we investigated the previously described GABI-KAT T-DNA line (GK-753B06; *c4h-4*; Schilmiller et al., 2009). In accordance with previous results the mutant showed seedling growth arrest (Fig. **1b**), with a strongly perturbed leaf development. Several growth parameters were quantified by growing *c4h-4* seedlings *in vitro* on ½ MS medium at 14 days after stratification (DAS). Compared to WT, mutant seedlings showed a reduction in primary root length and lateral root density (LRD) (Fig. **1c,d**), accompanied by an outgrowth of adventitious roots (ARs) at the root-hypocotyl junction.

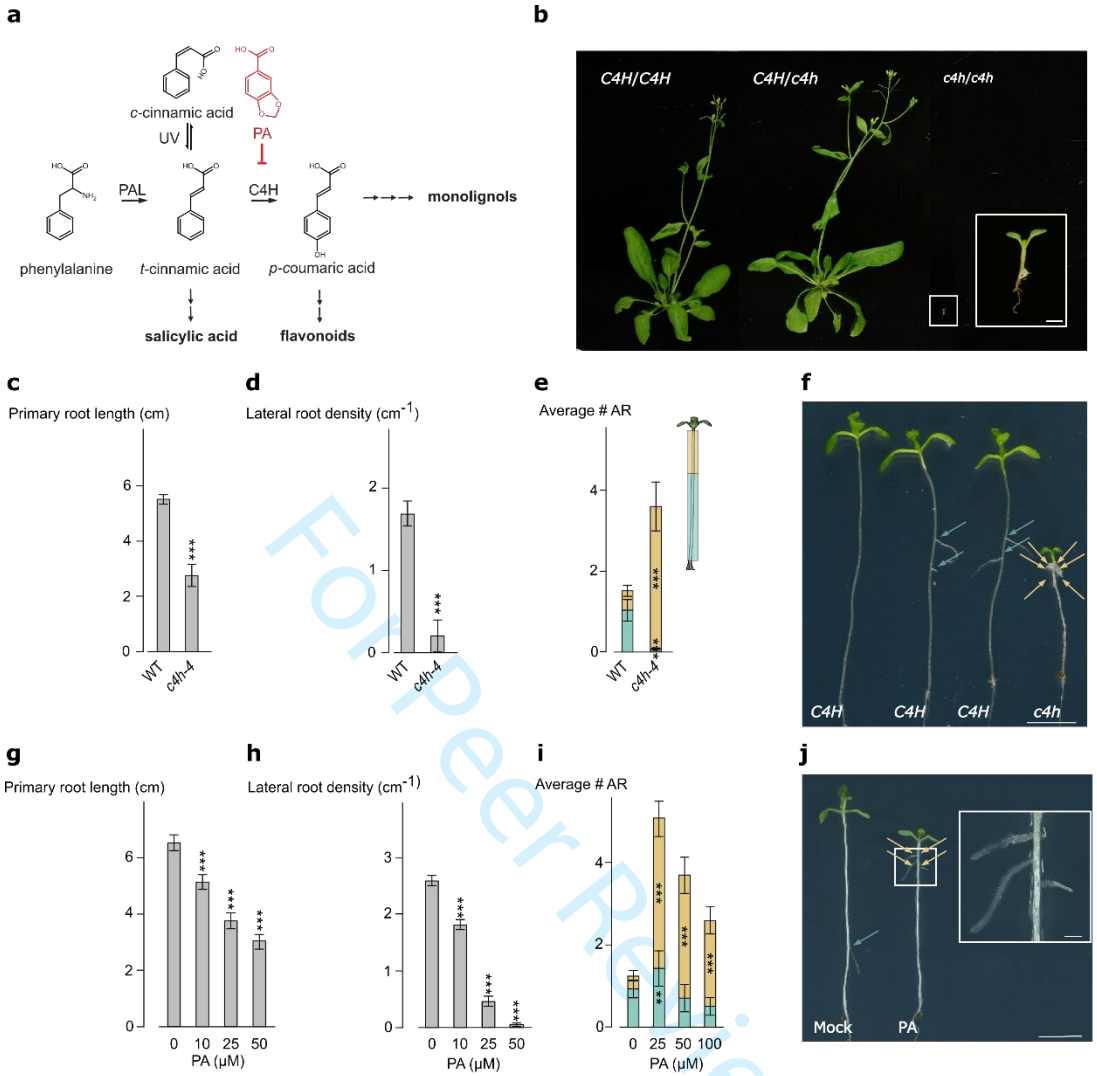

Figure 1.

To study the induction of the ARs in more detail, an AR-induction assay was implemented. This assay allows the analysis of the position of ARs along the length of the hypocotyl. Stratified wild type (WT) and *c4h-4* seeds were sown on ½ MS medium and given a light pulse before being stored in total darkness for seven days. The light pulse triggers germination and storing plants in darkness allows for etiolation of the hypocotyl. The plates with etiolated seedlings were subsequently transferred to long-day growth conditions, which allows for ARs outgrowth. After 7 days under long-day growth conditions adventitious rooting was assessed. *c4h-4* seedlings showed a significant increase in ARs number (Fig. **1e,f**) and, notably, the outgrowth of AR in the *c4h-4* seedlings was restricted almost primarily to the top third of the hypocotyl (Fig. **1e,f**).

As a result of its early growth arrest, the analysis of the *c4h-4* required the use of a segregating line, making its implementation in the experiments impractical. Therefore, for follow-up studies we chose to use piperonylic acid (PA), which is a well-described C4H-inhibitor (Schalk et al., 1998; Naseer et al., 2012; Van de Wouwer et al., 2016). Col-0 seeds were germinated on medium containing PA over a concentration range of 0-50 µM. At 14 DAS a dose-dependent reduction of both primary root length and LRD (Fig. **1g,h**) as well as an induction of ARs at the root-shoot junction were observed. These results are in line with the data obtained for the *c4h-4* mutant. Stratified Arabidopsis seeds were then etiolated on ½ MS medium containing a concentration range of PA (0-100 µM). Although to a lesser extent than the *c4h-4* mutant, seedlings treated with PA also showed a significant increase in ARs number (Fig. **1i,j**) in the apical region of the hypocotyl. Compared to the untreated control, the average number of ARs in the top third of the hypocotyl was significantly higher for all PA concentrations tested. In contrast, a slight increase of ARs in the lower section of the hypocotyl was only observed for 25 µM PA treated seedlings.

Overall, the data demonstrate that perturbation of C4H severely affects seedling development. This highlights the importance of a functional PPP during the early stages of plant growth, and validates its function in establishing early plant architecture.

2. Inhibition of C4H severely perturbs the PPP

C4H is active as the second enzyme in the PPP, and the entire flux through the pathway is shuttled via this step. Perturbing the function of C4H is therefore expected to have major consequences on the levels of PPP intermediates and end-products. To assess the effect of the inhibition of C4H on the metabolome of the plant, an LC-MS metabolite profiling of etiolated WT, *c4h-4* and PA-treated seedlings was performed (Table **1**). Both *c4h-4* and PA-treated seedlings showed an accumulation of compounds upstream of C4H (i.e. phenylalanine and products of cinnamic acid catabolism) and a depletion of products downstream of C4H (e.g. flavonoids and products leading to lignin building blocks). The results underline the pivotal role that C4H plays in the PPP, as exemplified by the severe perturbations in metabolite levels upon C4H inhibition, and

confirm C4H functionality to be strongly disrupted in both the *c4h-4* mutant and upon PA treatment. In addition, the shared phenotypes of the *c4h-4* mutant and PA-treated seedlings are reflected in the PCA plot of the metabolic profiles, with the *c4h-4* mutant and PA-treated seedlings clustering together (Fig. **2**). The slight disparity in clustering of the *c4h-4* mutant and PA could be explained by the differences in degree of pathway perturbation and the presence of PA and its catabolism products (Table **1**).

Together, these results confirm the pivotal role of C4H in secondary plant metabolism and prove the adequacy of PA-treatment as a substitute for the *c4h-4* mutation. The observed depletion in lignin building blocks is in line with previous observations in weaker *c4h* mutants (Schilmiller et al., 2009). The depletion in lignin is however difficult to reconcile with the observed developmental defects, including the specific apical induction of ARs. The latter has been rarely observed, but was previously linked to phytohormonal interplay (Rasmussen et al., 2017). Therefore, we further investigated the role of phytohormones in AR-induction upon inhibition of C4H.

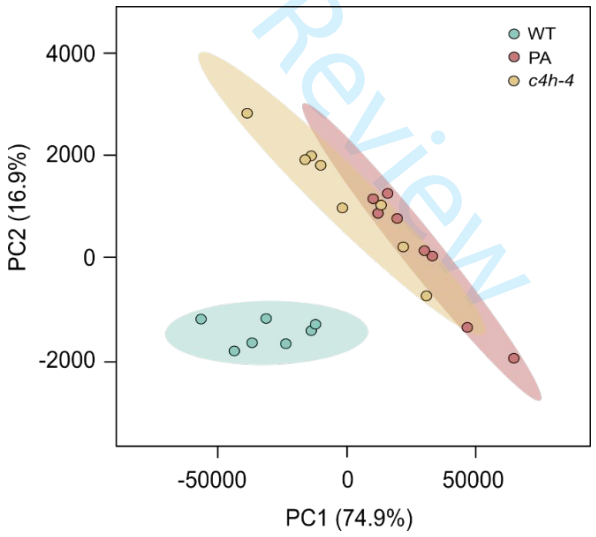

Figure 2.

Table 1.

No.	RT	m/z	Name	WT	*c4h-4*	Fold Change *c4h-4* - WT	PA	Fold Change PA - WT
			Phenylalanine and cinnamate derivatives					
1	2.19	164.0715	phenylalanine	20.25 ± 4.25	117.39 ± 28.03	5.80	48.97 ± 11.24	2.42
2	9.69	355.1028	cinnamoyl hexose (formic acid adduct)	0.61 ± 0.72	2215.55 ± 598.94	>100	1850.64 ± 604.39	>100
3	8.62	355.1028	cinnamoyl hexose (formic acid adduct)	0.49 ± 0.36	1125.18 ± 370.58	>100	1179.51 ± 441.18	>100
4	12.46	263.0550	cinnamoyl malate	0.00 ± 0.00	40.44 ± 12.27	>100	26.32 ± 7.96	>100
			Flavonoids					
5	6.93	623.1592	isorhamnetin glucoside rhamnoside 1	60.07 ± 19.24	0.00 ± 0.00	>100	1.45 ± 1.03	41.48
6	8.50	623.1603	isorhamnetin glucoside rhamnoside 2	1822.91 ± 532.53	0.44 ± 0.49	>100	128.30 ± 97.33	14.21
7	5.49	609.1447	kaempferol dihexoside	613.37 ± 139.24	0.00 ± 0.00	>100	16.63 ± 10.47	36.88
8	5.54	755.1994	kaempferol dihexoside rhamnoside 1	299.57 ± 81.86	0.03 ± 0.10	>100	26.81 ± 25.24	11.17
9	6.99	755.2016	kaempferol dihexoside rhamnoside 2	875.62 ± 217.82	0.00 ± 0.00	>100	9.07 ± 6.27	96.54
10	6.23	593.1481	kaempferol-3-O-a-L-rhamnopyranosyl(1,2)-b-D-glucopyranoside	55.62 ± 10.28	0.00 ± 0.00	>100	2.91 ± 3.93	19.11
11	8.08	739.2069	kaempferol-3-O-a-L-rhamnopyranosyl(1,2)-b-D-glucopyranoside-7-O-a-L-rhamnopyranoside 1	1436.33 ± 380.07	0.00 ± 0.00	>100	18.44 ± 23.38	77.90
12	6.22	739.2070	kaempferol-3-O-a-L-rhamnopyranosyl(1,2)-b-D-glucopyranoside-7-O-a-L-rhamnopyranoside 2	5768.48 ± 1279.59	8.53 ± 7.94	>100	486.21 ± 379.86	11.86
13	8.26	593.1498	kaempferol-rutinoside (hex+rha)	1389.46 ± 369.87	2.42 ± 2.68	>100	616.29 ± 626.08	2.25
			Ferulic acid derivatives					
14	7.24	551.1752	4/7/9-O-hexoside G(8-O-4)ferulic acid 1	130.59 ± 31.32	0.00 ± 0.00	>100	10.08 ± 3.35	12.95
15	7.58	551.1756	4/7/9-O-hexoside G(8-O-4)ferulic acid 2	161.06 ± 24.72	0.00 ± 0.00	>100	9.71 ± 3.54	16.59
16	5.94	551.1753	4/7/9-O-hexoside G(8-O-4)ferulic acid 3	210.85 ± 48.69	0.02 ± 0.05	>100	7.40 ± 2.52	28.49
17	6.98	551.1753	4/7/9-O-hexoside G(8-O-4)ferulic acid 4	390.72 ± 84.75	0.09 ± 0.11	>100	38.14 ± 11.76	10.24
18	6.70	551.1757	4/7/9-O-hexoside G(8-O-4)ferulic acid 5	1053.87 ± 177.17	0.00 ± 0.00	>100	83.44 ± 26.10	12.63
19	6.43	551.1759	4/7/9-O-hexoside G(8-O-4)ferulic acid 6	4063.76 ± 746.22	1.60 ± 1.90	>100	303.70 ± 82.14	13.38
24	4.07	371.0971	5-hydroxyferulic acid + hexose 1	70.56 ± 15.11	0.01 ± 0.02	>100	5.83 ± 2.28	12.10
25	3.60	371.0976	5-hydroxyferulic acid + hexose 2	375.78 ± 124.87	0.01 ± 0.04	>100	15.27 ± 7.95	24.61
26	5.96	339.1107	coniferaldehyde 4-O-hexoside	68.02 ± 20.82	3.07 ± 2.25	22.12	12.47 ± 7.74	5.45
27	3.84	387.1289	coniferin (formic acid adduct)	1932.65 ± 718.88	4.31 ± 2.75	>100	136.05 ± 68.97	14.21
28	3.20	357.1172	dihydroferulic acid + hexose	43.24 ± 12.28	0.01 ± 0.01	>100	0.02 ± 0.07	>100
29	11.34	535.1445	dihydroferuloyl-beta-keto acid + hexose + 136 Da	109.93 ± 31.85	0.00 ± 0.00	>100	26.80 ± 7.77	4.10
30	8.44	753.2220	disinapoyl hexose + hexose	134.27 ± 37.61	0.02 ± 0.05	>100	66.57 ± 59.17	2.02
31	3.72	355.1025	ferulic acid 4-O-hexoside 1	323.49 ± 55.67	0.12 ± 0.20	>100	20.92 ± 7.90	15.46
32	5.35	355.1029	ferulic acid 4-O-hexoside 2	1539.51 ± 379.00	1.07 ± 1.05	>100	48.18 ± 21.33	31.95
33	5.44	355.1029	ferulic acid 4-O-hexoside 3	2490.13 ± 485.84	19.86 ± 5.71	>100	253.94 ± 77.65	9.81
34	5.86	355.1027	feruloyl hexose	646.73 ± 146.47	0.08 ± 0.10	>100	10.75 ± 6.05	60.16
35	6.21	581.1845	feruloyl hexose + 226 Da 1	118.84 ± 32.12	0.25 ± 0.30	>100	12.92 ± 4.92	9.20
36	8.24	581.1856	feruloyl hexose + 226 Da 2	382.95 ± 93.27	0.00 ± 0.00	>100	21.58 ± 7.87	17.75
37	2.61	563.1600	feruloyl hexose 4-O-hexoside (formic acid adduct)	108.31 ± 30.85	0.19 ± 0.24	>100	13.17 ± 5.97	8.23
38	4.53	325.0919	feruloyl pentose 1	264.37 ± 112.58	45.61 ± 16.79	5.80	32.40 ± 12.72	8.16
39	5.10	325.0921	feruloyl pentose 2	456.51 ± 163.43	3.59 ± 1.77	>100	18.61 ± 8.00	24.54
40	5.92	583.2011	G 4-O-hexoside(8-O-4)G (formic acid adduct)	248.86 ± 94.48	0.00 ± 0.00	>100	0.08 ± 0.12	>100
41	10.13	533.1648	G(8-5)feruloyl hexose	264.64 ± 30.42	0.43 ± 0.44	>100	11.12 ± 4.03	23.80
42	9.20	519.1856	G(8-5)G hexoside	199.61 ± 62.44	0.00 ± 0.00	>100	0.40 ± 0.47	>100
43	8.19	469.0800	G(8-O-4)ferulic acid sulfate	841.14 ± 152.38	1.28 ± 2.49	>100	165.15 ± 91.89	5.09
44	10.32	389.1229	G(8-O-4)ferulic acid	105.31 ± 23.63	0.01 ± 0.02	>100	17.53 ± 4.92	6.01
45	10.25	505.1336	G(8-O-4)ferulic acid + malate	95.31 ± 22.14	0.24 ± 0.27	>100	15.27 ± 4.58	6.24
46	8.24	521.2011	G(red8-5)G + hexose 1	163.90 ± 28.32	0.00 ± 0.00	>100	0.60 ± 0.71	>100
47	9.08	521.2011	G(red8-5)G + hexose 2	715.41 ± 68.49	0.01 ± 0.03	>100	12.73 ± 7.75	56.21
49	5.54	385.1136	sinapic acid 4-O-hexoside 1	18148.45 ± 3185.04	276.41 ± 117.33	65.66	4779.87 ± 2163.07	3.80
50	6.10	385.1134	sinapic acid 4-O-hexoside 2	6030.09 ± 1234.35	74.89 ± 33.67	80.52	1623.39 ± 629.03	3.71
51	5.00	385.1129	sinapic acid 4-O-hexoside 3	161.43 ± 37.22	0.02 ± 0.05	>100	63.81 ± 23.86	2.53
52	4.39	385.1132	sinapic acid 4-O-hexoside 4	762.84 ± 139.35	5.45 ± 4.03	>100	304.76 ± 99.96	2.50
53	6.67	352.1029	sinapoyl glutamate 1	175.36 ± 48.08	1.79 ± 1.15	98.19	70.07 ± 26.78	2.50
54	6.03	352.1029	sinapoyl glutamate 2	248.59 ± 69.12	3.78 ± 2.11	65.72	101.05 ± 35.24	2.46
55	9.31	339.0715	sinapoyl malate 1	2921.54 ± 735.01	48.09 ± 25.75	60.76	1930.41 ± 595.57	1.51
56	9.01	339.0714	sinapoyl malate 2	3618.53 ± 554.83	67.86 ± 36.76	53.33	2349.53 ± 649.93	1.54
			PA derivatives					
57	9.52	165.0190	piperonylic acid	0.00 ± 0.00	0.04 ± 0.10	0.00	298.39 ± 82.70	>100
58	5.80	373.0769	piperonylic acid hexose (formic acid adduct)	0.90 ± 1.06	8.14 ± 19.46	9.05	5954.44 ± 2250.56	>100

3. Inhibition of C4H perturbs auxin transport

The induction and outgrowth of ARs are complex processes regulated by phytohormones, among which are jasmonate, ethylene and auxin (Gutierrez et al., 2012; Verstraeten et al., 2014; Steffens and Rasmussen, 2016; Lakehal and Bellini, 2019; Lakehal et al., 2019; Alallaq et al., 2020; Lakehal et al., 2020). The potential involvement of these phytohormones in AR spacing of *c4h* mutants was investigated using corresponding signaling mutants, namely *coi1-21* (jasmonate), e*tr1-3* (ethylene) and *tir1afb2afb3* (auxin). As PA-treated WT plants were shown to be an adequate substitute for the *c4h-4* mutant, AR growth was assessed for all signaling mutant lines upon treatment with and without 50 µM PA. Of the different lines tested, only the *tir1afb2afb3*

mutant did not show an increase in ARs upon PA treatment (Fig. **3a**). Additionally, the distribution of ARs along the hypocotyl upon PA treatment was unaffected in this mutant. These data show that PA-mediated AR-proliferation depends on the canonical auxin signaling pathway.

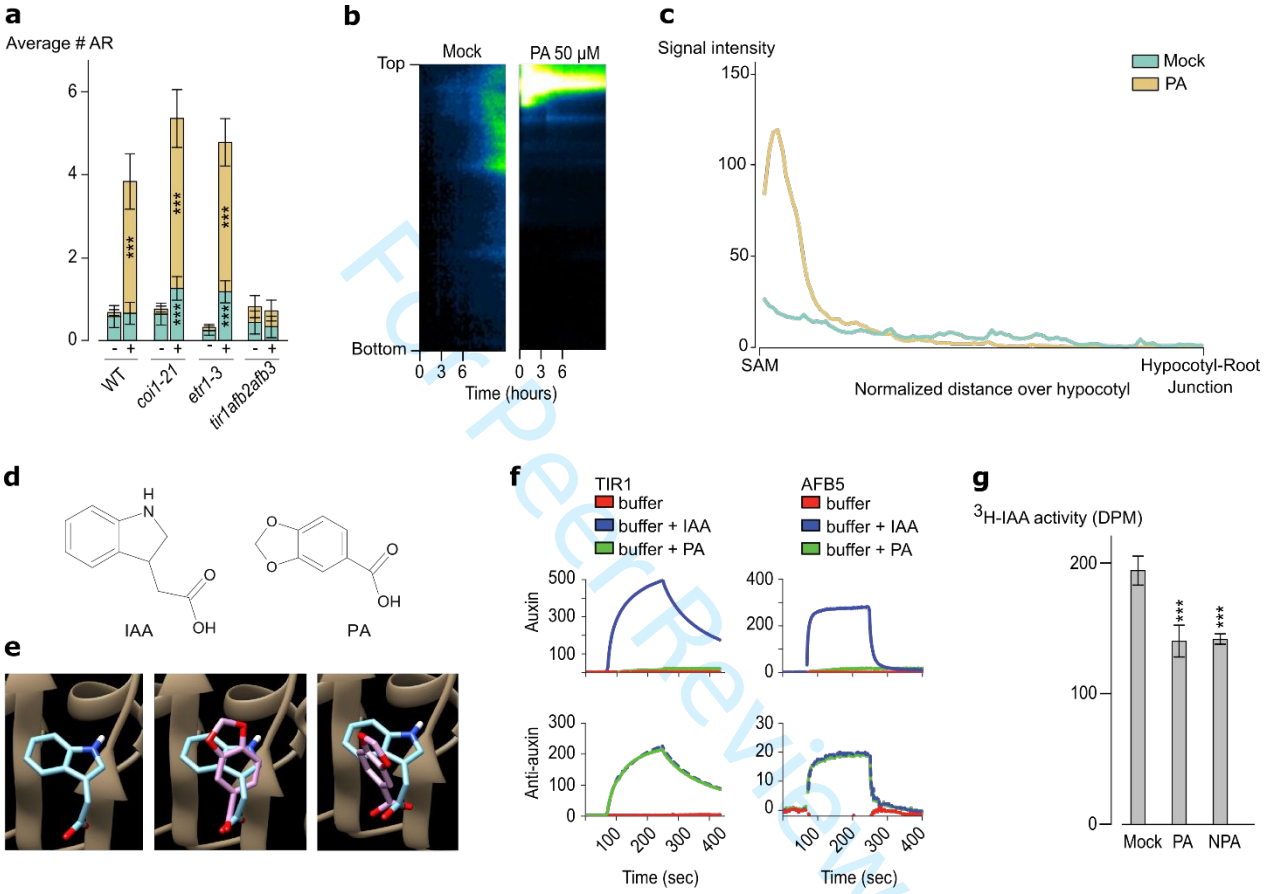

Figure 3.

To visualize the effect of PA on auxin distribution in the hypocotyl, seeds of the auxin reporter line *pDR5::LUC* were etiolated on medium supplemented with 50 µM PA. Luciferase activity was then followed in the hypocotyl by imaging the plants over a 12-hour time period, upon which a kymograph was generated (Fig. **3b**; (Xuan et al., 2015)). The kymograph revealed a strong apical accumulation of signal upon PA-treatment. Additionally, the signal intensity was lower in the basal parts of the hypocotyl compared to mock-treated hypocotyls. To obtain quantitative evidence, the *pDR5::LUC* signal was measured at the one-hour mark over the hypocotyl for 50 hypocotyls treated with/without

50 μM PA. Upon PA treatment, a strong apical accumulation of signal was observed in the apical third of the hypocotyl that dropped to near zero for the basal two-thirds (Fig. **3c**). This was in contrast with the mock-treated plants, which showed a steady decline in signal from the top to the bottom of the hypocotyl. These results indicate that inhibition of C4H perturbs auxin homeostasis, most likely by affecting auxin transport.

It could be hypothesized that PA itself activates the auxin signaling cascade in the reporter lines by binding to an auxin receptor. After all, PA and IAA are similar in size (166 Da and 175 Da, respectively) and share a planar aromatic skeleton decorated with a carboxylic acid characteristic for auxins ((Veldstra, 1953); Fig. **3d**). However, despite the similarities, the carbon skeletons differ, with PA being a benzodioxane and IAA an indole, and the length of the side chains is different. In line with these structural dissimilarities, molecular docking of PA in the binding pocket of the auxin receptor TIR1 showed it to adopt a pose distinctly out of alignment with the pose of IAA (Fig. **3e**), making it unlikely that PA itself can activate auxin signaling. Confirming evidence was obtained via Surface Plasmon Resonance (SPR), where interaction kinetics of PA with either TIR1 or the related auxin receptor AFB5 were followed. Hereby, no evidence was found that PA could bind either the TIR1 or AFB5 receptor, showing that it is neither an auxin nor an antiauxin (Fig. **3f**).

Next we quantified auxin transport in etiolated seedlings grown on medium supplemented with or without 50 μM PA. Treatment with the auxin transport inhibitor *N*-1-naphthylphthalamic acid (NPA) was included as a positive control. This experiment revealed that the auxin transport capacity measured upon treatment with both PA and NPA was significantly reduced when compared to that of mock-treated plants (Fig. **3g**). Together, these results indicate that inhibition of C4H affects auxin homeostasis in the hypocotyl via the inhibition of auxin transport.

4. Auxin transport inhibition upon blocking C4H is partially caused by *c*-CA accumulation

The perturbation of auxin transport upon inhibition of C4H could find its origin in the accumulation of bioactive molecules derived from compounds upstream of C4H.

342 Interestingly, two such molecules have been described as having auxin transport
343 regulatory properties: *cis*-cinnamic acid (*c*-CA) being an auxin transport inhibitor
344 Steenackers et al., 2019) and salicylic acid being an auxin transport modulator (Tan et al.,
345 2020).
346

347

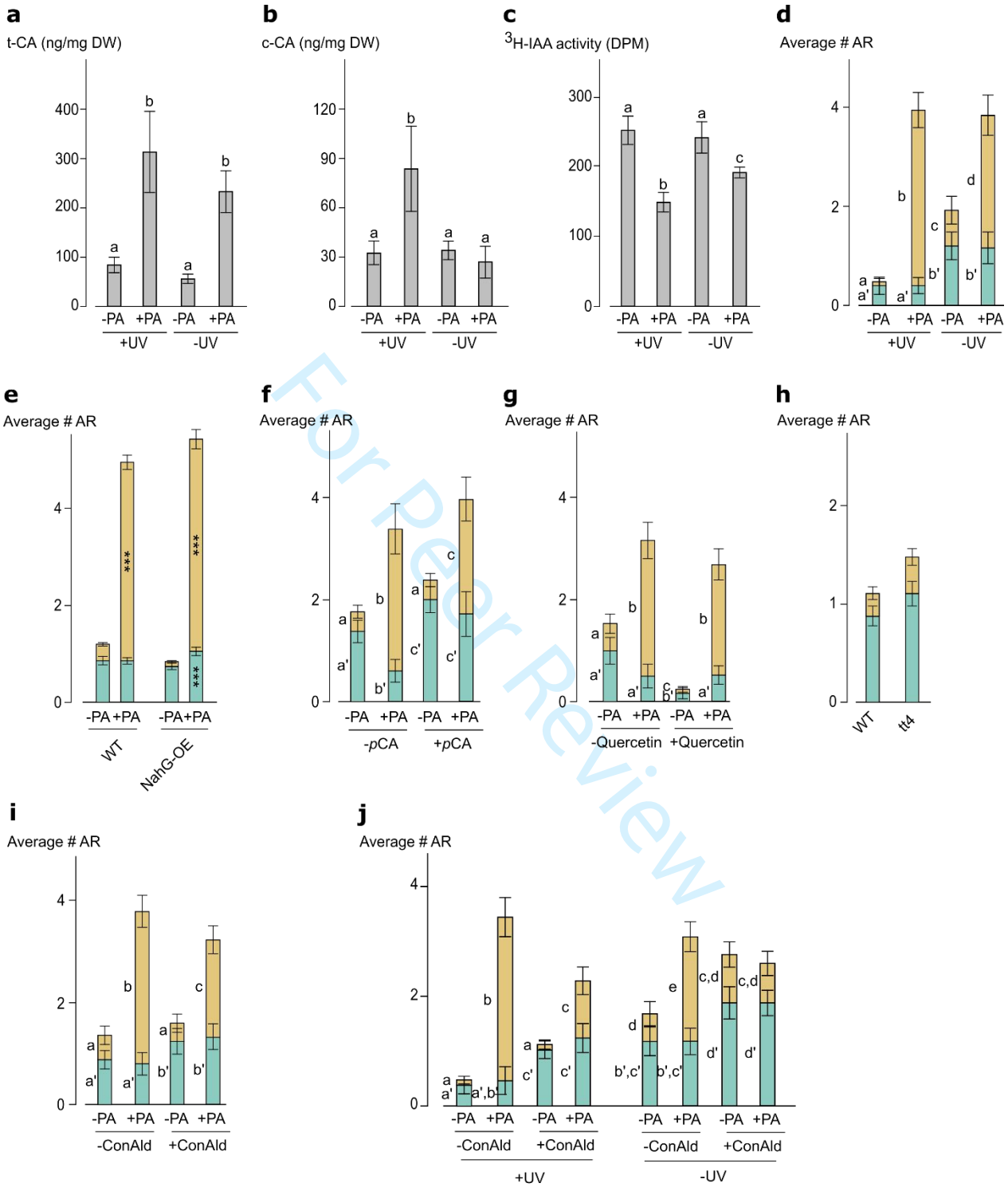

348 **Figure 4.**

349

c-CA is the UV-mediated isomerization product of the C4H substrate *trans*-cinnamic acid (*t*-CA) (Wong et al., 2005; Steenackers et al., 2019). Our metabolomic profiling upon PA treatment showed the accumulation of conjugation products of cinnamic acid (Table **1**), suggesting that cinnamic acid itself accumulates upon inhibition of C4H. Moreover, because all experiments had been conducted under growth conditions containing UV-light, the accumulation of *c*-CA might explain the observed phenotypes. According to this hypothesis, growing PA-treated plants under UV-free light should reduce the *c*-CA content and attenuate the growth phenotypes. Despite the assumed requirement of UV-light to form *c*-CA, basal levels of both CA isomers were detected in mock-treated seedlings grown under both light with and without UV. Treatment with PA significantly increased *t*-CA-levels for both light conditions (Fig. **4a**), but *c*-CA levels were increased only under light containing UV (Fig. **4b**). Thus, besides the indication for an as of yet unknown UV-independent mechanism for plants to produce *c*-CA, the data revealed that UV increases *c*-CA levels in PA-treated seedlings.

If *c*-CA is indeed the causal agent for the PA-triggered perturbation of auxin transport, avoiding *c*-CA accumulation by growing PA-treated seedlings under light without UV should restore auxin transport. To investigate this, auxin transport was quantified for plants grown under light with and without UV (Fig. **4c**). In mock-treated plants auxin transport capacity was not significantly different for both light conditions. PA on the other hand significantly decreased auxin transport capacity for both light treatments, although not to the same extent. Auxin transport was significantly more inhibited for PA-treated plants grown under UV-light as compared to plants grown under light without UV. The dependency of PA on UV-light to inhibit auxin transport is in line with the proposed model indicating the involvement of *c*-CA as an auxin transport inhibitor. However, the mild but significant inhibition of auxin transport upon PA-treatment under UV-free conditions was unexpected as *c*-CA levels were not increased in these plants. These data suggest that, in addition to *c*-CA, other players are involved in the auxin transport inhibition upon blocking of C4H.

In order to determine whether the light-dependent variations in auxin transport translate to phenotypic changes, AR growth was assessed under both light conditions (Fig. **4d**). Changing light conditions did not affect the total number of ARs formed upon

PA treatment over the entire hypocotyl. However, the distribution of AR over the hypocotyl was altered, as UV-grown plants showed a significantly higher increase in ARs in the top part of the hypocotyl upon PA treatment. This indicates that *c*-CA has a partial involvement in the outgrowth of ARs in the top part of the hypocotyl upon PA-treatment. These results are in line with the auxin transport measurements, showing an effect of PA that is more pronounced in plants grown in UV-containing light. However, the lack of a full complementation of the PA-phenotype upon preventing *c*-CA accumulation further supports the hypothesis that besides *c*-CA other players are involved in the PA-triggered AR phenotypes.

Salicylic acid, which is also produced upstream of C4H, has also been described as an auxin transport modulator (Zhao et al., 2015; Tan et al., 2020). To test the potential involvement of salicylic acid in the PA-mediated perturbation of auxin homeostasis, we assessed AR growth for the *NahG-OE* Arabidopsis line (Gaffney et al., 1993) upon treatment with and without 50 µM PA. The *NahG-OE* line encodes a salicylate hydroxylase that catabolizes salicylic acid, thus inactivating it. Upon PA-treatment, *NahG-OE* plants showed an accumulation of AR in the top third similar to that of the WT (Fig. **4e**), refuting the involvement of salicylic acid in affecting auxin homeostasis upon PA-treatment.

5. *c*-CA accumulation and a depletion in monolignols: a dual mechanism at play

Besides accumulation of upstream compounds, the inhibition of C4H causes a depletion of products downstream of C4H (Table 1), which could also explain part of the phenotypes. To identify whether the depletion of a compound downstream of C4H is responsible for the observed inhibition of auxin transport in PA-treated seedlings, a co-treatment was performed with 50 µM PA and 200 µM *p*-coumaric acid (*p*CA), which is the product of C4H. The co-treatment did not lead to a decrease in total AR formation (Fig. **4f**). Interestingly however, there was a significant drop in ARs in the apical third of the hypocotyl compared to plants treated with PA only (Fig. **4f**), suggesting that a player downstream of C4H is involved.

One group of molecules downstream of C4H known to modulate auxin transport are the flavonoids, among which quercetin is one of the most well-studied (Peer and

412 Murphy, 2007). Our previous metabolomic profiling of PA-treated etiolated seedlings
413 showed a strong depletion in flavonoid content. To assess whether a depletion of
414 quercetin could account for the AR phenotype a co-treatment of 50 µM PA with 100 µM
415 quercetin was performed. Co-treatment with quercetin did not result in complementation
416 of AR growth or distribution (Fig. **4g**), suggesting that it is not involved. As quercetin is not
417 the only flavonoid known to modulate auxin transport, a *tt4* mutant deficient in the
418 production of flavonoids (Brown et al., 2001) was analyzed alongside a WT control. The
419 *tt4* mutant did not show a significant increase in ARs in the top third of the hypocotyl (Fig.
420 4H), suggesting that flavonoids are not the downstream factor involved in the growth
421 defects upon inhibition of C4H.

422 As the majority of the carbon entering the phenylpropanoid pathway is incorporated
423 into lignin, blocking the pathway has a strong negative effect on the lignin content (Van
424 de Wouwer et al., 2016). To examine whether a depletion of lignin is causal to the
425 phenotypes, we repeated the complementation assays with 100 µM coniferaldehyde
426 (ConAld), which was chosen for this purpose based on its stability under light and it being
427 a precursor to both the S- and G-units that constitute the majority of the lignin polymer
428 (Boerjan et al., 2003). In accordance to the co-treatment with *p*CA, co-treatment with
429 ConAld partially restored the number and distribution of ARs in PA-treated etiolated
430 seedlings (Fig. **4i**). These results strongly indicate a depletion of monolignols to be
431 involved in the phenotypes induced upon inhibition of C4H.

432 Both co-treatment with PA and ConAld as well as growing PA-treated seedlings
433 under UV-free light partially complemented the adventitious rooting phenotype. It was
434 therefore assessed whether the treatments act additively. For this purpose, seedlings
435 were etiolated on medium with or without 50 µM PA and 100 µM ConAld and grown under
436 light with or without UV (Fig. **4j**). Upon co-treatment with ConAld under UV-free light
437 conditions, PA did not significantly change the number nor the distribution of ARs.
438 Together these results show that a dual mechanism is at play for the establishment of the
439 AR phenotypes upon inhibition of C4H, with both an accumulation of *c*-CA and a depletion
440 in monolignols involved.
441
442

6. Lignin depletion perturbs long-distance auxin transport

The depletion of monolignols was shown to explain part of the developmental defects upon C4H inhibition, suggesting that lignin is crucial for proper seedling development. We therefore assessed whether the phenotypic restoration upon co-treatment with ConAld corresponded to a restoration in auxin distribution. For this purpose, seeds of the auxin reporter line *pDR5::LUC* were etiolated on medium supplemented with or without 50 µM PA and 100 µM ConAld. The intensity of the *pDR5::LUC* signal was then measured over the hypocotyl. Mock-treated plants showed a steady decline in signal from the top to the bottom of the hypocotyl, and upon PA treatment a strong apical accumulation of signal was again observed in the apical third of the hypocotyl (Fig. **5a**). Co-treatment of PA with ConAld significantly decreased the apical accumulation of signal, hereby partially complementing the perturbation in auxin distribution. These results are thus in line with the phenotypic data, and signify that lignin deposition is vital for the correct distribution of auxin over the plant.

458

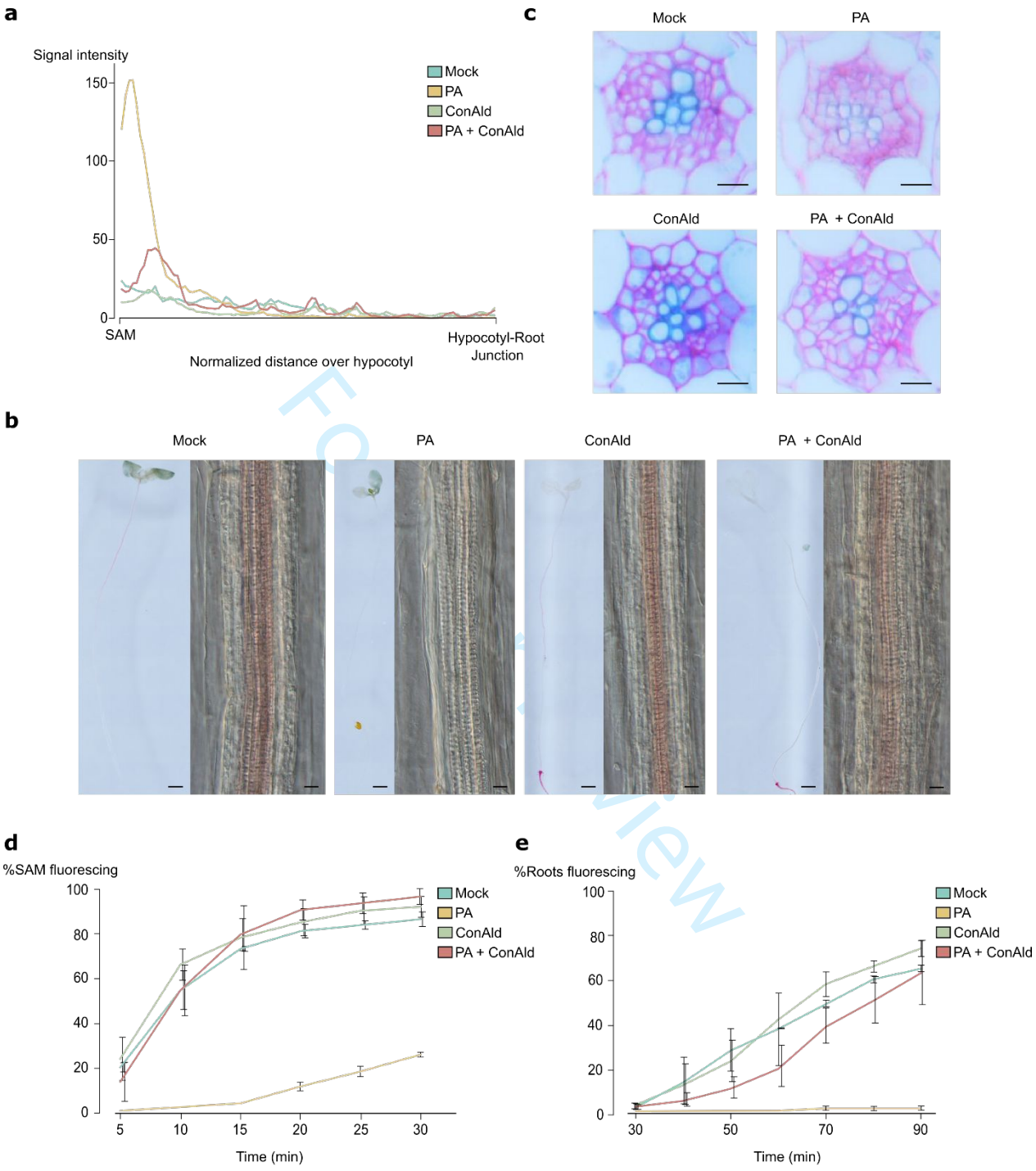

459 **Figure 5.**

460

461 To further assess the involvement of lignin in the observed phenotypes,
462 Arabidopsis seedlings were etiolated on medium with or without 50 μM PA and 100 μM
463 ConAld. Lignin distribution was visualized by Wiesner staining. Whereas seedlings treated

with PA showed a strongly reduced staining in the vascular tissue, staining in this region was partially complemented for upon co-treatment with ConAld (Fig. **5b**). Hypocotyl cross-sections were stained with toluidine blue to visualize lignin and counterstained with ruthenium red to visualize the plant cell walls. This revealed a reduced blue staining in the xylem vessels upon PA treatment, which pointed towards a reduced lignin content in these cells (Fig. **5c**). In line with the Wiesner staining, the reduced lignin content was partially complemented for upon co-treatment with ConAld.

To correlate these observations to xylem functionality, we assessed xylem transport capacity in the hypocotyl using 5(6)-carboxyfluorescein diacetate (CFDA; (Melnyk et al., 2015)). Arabidopsis seedlings were etiolated on medium with or without 50 µM PA and 100 µM ConAld. The hypocotyl was cut above the root-hypocotyl junction and a droplet of CFDA was applied at the base of the hypocotyl. The presence of the fluorescent signal was then monitored over time in the shoot apical meristem (SAM). Whereas fluorescence observed in the SAM rapidly increased for mock-treated hypocotyls (Fig. **5d**) this occurred at a much later time point for the PA-treated seedlings. Additionally, only a fraction of the PA-treated hypocotyls showed fluorescence in the SAM after 30 minutes. Xylem transport capacity was fully restored upon co-treatment of PA with ConAld, showing that the partial complementation of lignin in the xylem observed previously is sufficient for a restoration of xylem functionality.

The perturbed xylem functionality could explain for the auxin transport inhibition via the Münch model (Munch, 1930; Knoblauch et al., 2016). Long-distance auxin transport is known to occur via the phloem, and the Münch model proposes phloem transport to be driven by a pressure gradient generated at the top of the plant. This gradient is established by the upward transport of water via the xylem, meaning that a defect in xylem transport could lead to a perturbed phloem and therefore auxin transport. To test this hypothesis, phloem transport capacity was assessed in etiolated seedlings using CFDA. Arabidopsis seedlings were etiolated on medium with or without 50 µM PA and 100 µM ConAld. A droplet of CFDA was applied to the cotyledons, upon which the fluorescent signal was monitored over time in the root-hypocotyl junction (Fig. **5e**). In contrast to the mock-treated hypocotyls, only 1% of the PA-treated seedlings showed fluorescence in the root-shoot junction at the final time point. Analogous to the xylem transport, co-treatment of PA with

ConAld complemented the phloem transport capacity, showing that the adequate deposition of lignin is required for proper phloem transport.

7. Confirmation of results in the *c4h-4* mutant

To obtain conclusive evidence that the inhibition of C4H leads to the inhibition of long-distance auxin transport, key experiments were repeated using the heterozygous *c4h-4* mutant. AR growth was assessed for WT and the segregating *c4h-4* mutant seeds upon treatment with or without 100 µM ConAld. As expected, treatment of the segregating *c4h-4* mutant population with 100 µM ConAld resulted in substantial phenotypic complementation, which encumbered identification of the homozygous *c4h-4* seedlings. The seedlings were therefore genotyped to identify the homozygous mutants. Analogous to PA-treated seedlings, etiolated homozygous *c4h-4* mutant plants treated with ConAld showed a significant complementation of AR-growth in the top third of the hypocotyl (Fig. **6a**). These results thus confirm the inhibition of C4H and subsequent depletion in monolignols to be causal to the increased AR induction and their specific apical spacing, hereby again showing the requirement of lignin deposition in the establishment of auxin distribution in seedlings.

512

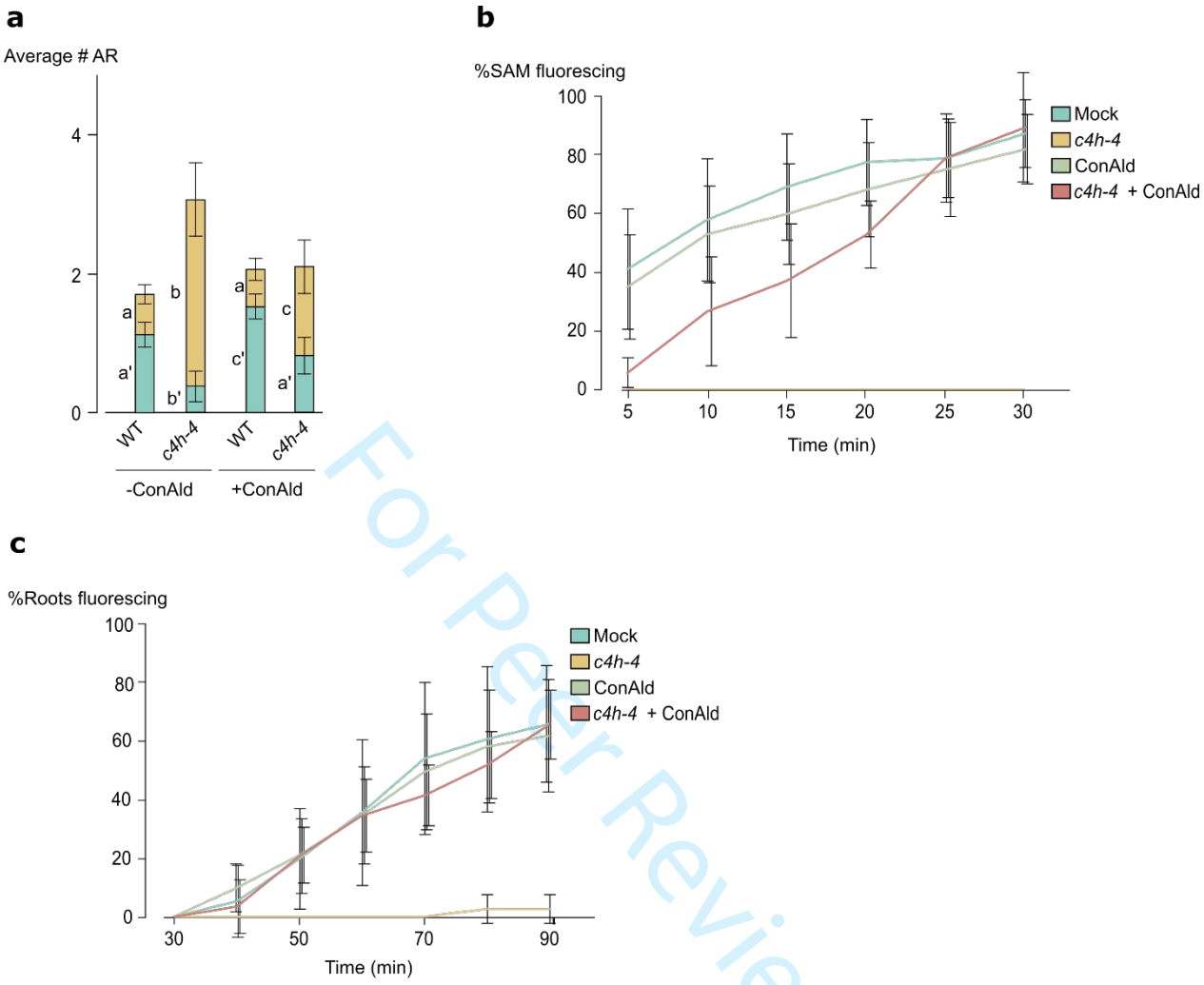

513 **Figure 6.**

514 To confirm the involvement of the vascular tissue and thus long-distance auxin
515 transport in the establishment of these phenotypes, we repeated the xylem and phloem
516 transport assays using the *c4h-4* mutant. Seeds from Col-0 WT and a segregating
517 seedstock of the *c4h-4* mutant were etiolated on medium supplemented with or without
518 100 µM ConAld. Xylem transport was assessed as described above using the fluorescent
519 tracker CFDA. Homozygous *c4h-4* mutants were afterwards identified by genotyping.
520 Similar to PA treatment, the *c4h-4* mutant showed a severely perturbed xylem functionality
521 (Fig. **6b**). Treatment of the *c4h-4* mutant with ConAld significantly restored xylem
522 transport, although transport velocity appeared slower than for the Col-0 WT. Phloem
523 transport was assessed as described above for etiolated Col-0 WT and the segregating

524 *c4h-4* mutant treated with or without 100 µM ConAld. Homozygous *c4h-4* mutants were
525 afterwards identified by genotyping. Again, results were analogous to those obtained for
526 PA-treated seedlings, with phloem transport being almost entirely perturbed in the *c4h-4*
527 mutant (Fig. **6c**) and treatment with ConAld completely restoring phloem transport in the
528 mutant.

529 Together, these results indicate that a two-fold mechanism comprising both a
530 depletion in lignin and an accumulation of *c*-CA lie at the basis of auxin transport inhibition
531 upon blocking C4H (Fig. **7**). As such, the requirement of a functional PPP and lignin
532 deposition in the establishment of auxin transport and homeostasis in plants is illustrated.
533 Hereby, we demonstrate the role of the PPP in the determination of plant development
534 and architecture.

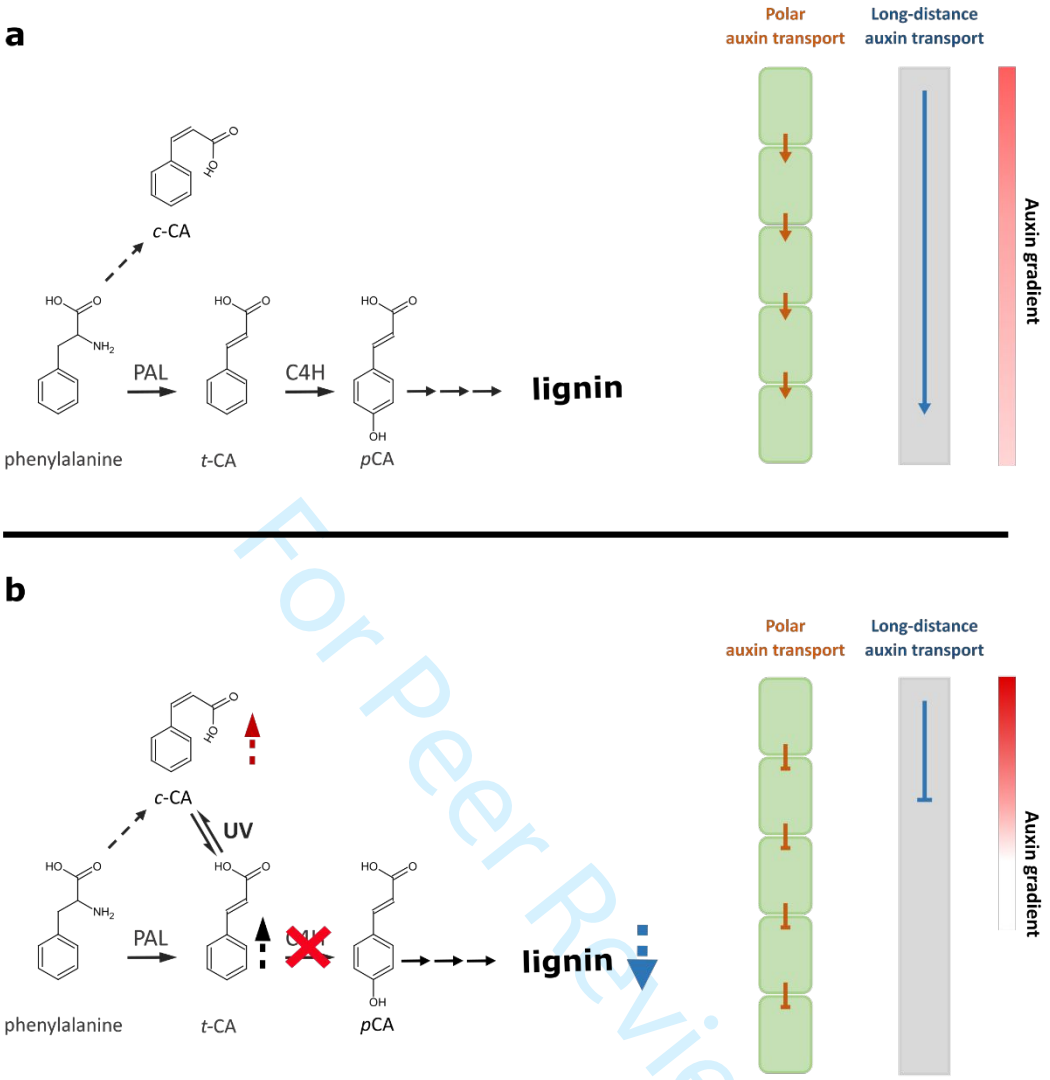

Figure 7.

DISCUSSION

Inhibiting the function of C4H in Arabidopsis seedlings either in the *c4h-4* mutant or upon PA treatment resulted in severe and distinct phenotypes, with an impeded lateral root development and a strong accumulation of adventitious roots specifically in the apical part of the hypocotyl. These phenotypes were found to be caused by a perturbation in auxin transport, resulting in the accumulation of auxin apically in the hypocotyl. The underlying cause of the perturbation in auxin homeostasis was found to be two-fold, namely by a downstream depletion in lignin and presumably by the upstream accumulation of the endogenous auxin transport inhibitor *c*-CA.

c-CA was previously presumed to be produced via isomerization of *t*-CA under exposure to UV light (Wong et al., 2005; Steenackers et al., 2019). However, we here found *c*-CA to also be present in plants grown under UV-free conditions. Additionally, the levels of *c*-CA present in the mock-treated plant were similar for UV- and UV-free-grown plants. This points towards a UV-independent biosynthesis route toward *c*-CA, possibly via a dedicated enzymatic biosynthesis. Upon inhibition of C4H there is a strong accumulation of *t*-CA. This accumulation of *t*-CA is however only accompanied by an increase in *c*-CA in UV-grown plants. When C4H is inhibited in UV-free-grown plants there is a strong accumulation in levels of *t*-CA only. As without UV the excess in *t*-CA does not result in an increase in *c*-CA levels, it appears that the biosynthesis of *c*-CA is independent of *t*-CA. A possible biosynthesis route towards *c*-CA could be directly from phenylalanine. Together, the presented results help us in further understanding the role of *c*-CA as an endogenous plant growth regulator.

By further dissecting the underlying molecular causes of the phenotypes, the involvement of other pathway intermediates and end products that are known auxin transport modulators (salicylic acid, flavonoids) was refuted (Tan et al., 2020; Peer and Murphy, 2007). Our findings indicated lignin deposition as an indirect requirement for phloem-mediated auxin transport. The drop in lignin content when blocking the PPP alters auxin homeostasis resulting in the developmental defects. Lignin deposition is however known to occur in the xylem but not the phloem vessels, pointing towards the perturbation in xylem functionality as a primary cause of effect. Although we cannot exclude alternative hypotheses, the adverse effect of xylem transport perturbation on phloem transport capacity as explained by the Münch model seems most likely (Munch, 1930; Knoblauch et al., 2016). This states that phloem transport is driven by a pressure gradient generated at the apical part of the plant. This gradient is established by the transport of water via the xylem. Impaired lignification would thus disrupt xylem functionality and, indirectly, also phloem transport. As an altered lignin content of the xylem has been described for numerous PPP mutants (Vanholme et al., 2019b), it is likely that phloem transport is also affected in these mutants. An impairment in auxin transport and phloem transport could explain some of the phenotypes observed in PPP mutants. For example, many PPP mutants show dwarfism and a lack of apical dominance (Hoffmann et al., 2004; Schilmiller

et al., 2009; Bonawitz and Chapple, 2013; De Meester et al., 2018). Whereas the reduction in plant height is considered a direct consequence of a perturbed water transport, the loss of apical dominance could be a consequence of an impaired auxin transport capacity. In addition, the transport of solutes and sugars that typically occurs via the phloem will be affected. Disturbing transport of these solutes would effectively disrupt the efficient distribution of energy throughout the plant, further contributing to the stunted growth of some of these mutants.

Auxin transport inhibition has been previously proposed to cause the growth defects of an *HCT-RNAi* line (Besseau et al., 2007). The growth defects in this *hct* mutant were linked to the upstream accumulation of flavonoids, which were presumed to cause an observed inhibition in auxin transport. Reducing flavonoid content in the *hct* mutant by silencing *CHS,* which is involved in flavonoid production, indeed went paired with a restoration of both growth and auxin transport. However, in a later study, the growth defects observed in the *hct* mutant were found to be independent of flavonoids (Li et al., 2010). Here, the authors pointed towards a slight restoration in lignification in the *chs/hct* double mutant compared to the *hct* line to allow for the growth restoration. Indeed, low levels of lignin deposition seem to allow already for a large portion of plant growth. This is illustrated by the much stronger growth perturbation of the *c4h-4* knock-out mutant compared to partial *c4h* loss-of-function mutants (*ref3-1*, *ref3-2* and *ref3-3*; (Schilmiller et al., 2009)). However, a possible link between the increase in lignin content and the restoration in auxin transport in the *chs/hct* mutant was so far not investigated for. If auxin transport inhibition in the *hct* mutant was also caused by a defective lignification, the observed restoration of auxin transport in the *chs/hct* mutant would thus also be caused by the small restoration of lignification and not the reduction in flavonoid content.

As lignin hinders the efficient conversion of plant biomass to fermentable sugars, reducing lignin content in plants is part of ongoing strategies to optimize plant biomass for a more efficient processing (Vanholme et al., 2013). Understanding the phenotypes associated with lowering lignin content in plants is therefore a prerequisite in the light of these valorization purposes. Previously, phenotypes of PPP mutants were hypothesized to be caused by either an accumulation of products upstream or a depletion of products downstream in the pathway (Muro-Villanueva et al., 2019). Here we show that in the case

of C4H both models contribute, as polar auxin transport inhibition is caused by the accumulation of *c*-CA, and long-distance auxin transport is inhibited by a depletion of lignin. Remarkably, both models contribute to the same phenotype, namely the apical accumulation of ARs. Nevertheless, as phenylpropanoids are involved in a wide range of physiological processes, the phenotypes induced by accumulating compounds are expected to be different for each PPP mutant. By thus charting a role for both the accumulation and depletion of PPP intermediates in the establishment of the phenotypes upon inhibition of C4H, this research improves our understanding of the underlying factors contributing to the growth phenotypes of PPP mutants. Particularly, by establishing a role for lignin already at the early seedling stage, we demonstrate a fundamental position for lignin apart from providing plant rigidity linked to upright growth. These observations thus have clear implications pertaining the ongoing strategies to engineer the phenylpropanoid pathway towards a more efficient bio-based economy.

ACKNOWLEDGEMENTS

This work was supported by the Fonds voor Wetenschappelijk Onderzoek – Vlaanderen (FWO) through project number G008116N and personal grants to I.E.H. (1S04020N) and C.V.B. (11D8220N). R.N. acknowledges the support of BBSRC award BB/L009366/1. Part of the work was performed by I.E.H at the Sainsbury Laboratory, University of Cambridge funded by the European Molecular Biology Organization (EMBO; STF-8658). We would like to thank prof. Ottoline Leyser for hosting performance of these experiments and dr. Martin van Rongen and dr. Sally Ward for technical advice. We would also like to thank the VIB Metabolomics Core Facility and Geert Goeminne for processing of the LC-MS samples.

AUTHOR CONTRIBUTIONS

I.E.H., A.C., R.N., T.B., J.F., B.D.R., W.B. and B.V. designed the experiments. I.E.H., C.V.B., H.E.A., H.H., J.P., W.S. and M.Q. performed the experiments. V.S. and J.P. contributed new tools. I.E.H. and B.V. wrote the manuscript.

638

639 **REFERENCES**

640

641 Abdulrazzak, N., Pollet, B., Ehlting, J., Larsen, K., Asnaghi, C., Ronseau, S., Proux, C., Erhardt,
642 M., Seltzer, V., and Renou, J.-P. (2006). A coumaroyl-ester-3-hydroxylase insertion mutant
643 reveals the existence of nonredundant meta-hydroxylation pathways and essential roles for
644 phenolic precursors in cell expansion and plant growth. Plant Physiology 140, 30-48.
645 Alallaq, S., Ranjan, A., Brunoni, F., Novák, O., Lakehal, A., and Bellini, C. (2020). Light controls
646 de novo adventitious root regeneration by modulating jasmonate and cytokinin homeostasis
647 in Norway spruce hypocotyls. bioRxiv.
648 Besseau, S., Hoffmann, L., Geoffroy, P., Lapierre, C., Pollet, B., and Legrand, M. (2007).
649 Flavonoid accumulation in Arabidopsis repressed in lignin synthesis affects auxin transport
650 and plant growth. The Plant Cell 19, 148-162.
651 Boerjan, W., Ralph, J., and Baucher, M. (2003). Lignin biosynthesis. Annual review of plant
652 biology 54, 519-546.
653 Bonawitz, N.D., and Chapple, C. (2013). Can genetic engineering of lignin deposition be
654 accomplished without an unacceptable yield penalty? Current opinion in biotechnology 24,
655 336-343.
656 Bonawitz, N.D., Im Kim, J., Tobimatsu, Y., Ciesielski, P.N., Anderson, N.A., Ximenes, E., Maeda,
657 J., Ralph, J., Donohoe, B.S., and Ladisch, M. (2014). Disruption of Mediator rescues the
658 stunted growth of a lignin-deficient Arabidopsis mutant. Nature 509, 376-380.
659 Brown, D.E., Rashotte, A.M., Murphy, A.S., Normanly, J., Tague, B.W., Peer, W.A., Taiz, L., and
660 Muday, G.K. (2001). Flavonoids act as negative regulators of auxin transport in vivo in
661 Arabidopsis. Plant physiology 126, 524-535.
662 Brunetti, C., Fini, A., Sebastiani, F., Gori, A., and Tattini, M. (2018). Modulation of phytohormone
663 signaling: a primary function of flavonoids in plant–environment interactions. Frontiers in
664 plant science 9, 1042.
665 Chong, J., Poutaraud, A., and Hugueney, P. (2009). Metabolism and roles of stilbenes in plants.
666 Plant science 177, 143-155.

667 Coleman, H.D., Samuels, A.L., Guy, R.D., and Mansfield, S.D. (2008). Perturbed lignification
668 impacts tree growth in hybrid poplar—a function of sink strength, vascular integrity, and
669 photosynthetic assimilation. Plant Physiology 148, 1229-1237.
670 De Meester, B., de Vries, L., Özparpucu, M., Gierlinger, N., Corneillie, S., Pallidis, A., Goeminne,
671 G., Morreel, K., De Bruyne, M., and De Rycke, R. (2018). Vessel-specific reintroduction
672 of cinnamoyl-COA reductase1 (CCR1) in dwarfed ccr1 mutants restores vessel and xylary
673 fiber integrity and increases biomass. Plant physiology 176, 611-633.
674 De Smet, I., Chaerle, P., Vanneste, S., De Rycke, R., Inzé, D., and Beeckman, T. (2004). An easy
675 and versatile embedding method for transverse sections. Journal of microscopy 213, 76-80.
676 Dharmasiri, N., Dharmasiri, S., Weijers, D., Lechner, E., Yamada, M., Hobbie, L., Ehrismann, J.S.,
677 Jürgens, G., and Estelle, M. (2005). Plant development is regulated by a family of auxin
678 receptor F box proteins. Developmental cell 9, 109-119.
679 Dolan, W.L., Dilkes, B.P., Stout, J.M., Bonawitz, N.D., and Chapple, C. (2017). Mediator Complex
680 Subunits MED2, MED5, MED16, and MED23 Genetically Interact in the Regulation of
681 Phenylpropanoid Biosynthesis. The Plant cell 29, 3269-3285.
682 Franke, R., Hemm, M.R., Denault, J.W., Ruegger, M.O., Humphreys, J.M., and Chapple, C.
683 (2002). Changes in secondary metabolism and deposition of an unusual lignin in the ref8
684 mutant of Arabidopsis. The Plant Journal 30, 47-59.
685 Gaffney, T., Friedrich, L., Vernooij, B., Negrotto, D., Nye, G., Uknes, S., Ward, E., Kessmann, H.,
686 and Ryals, J. (1993). Requirement of salicylic acid for the induction of systemic acquired
687 resistance. Science 261, 754-756.
688 Gallego-Giraldo, L., Escamilla-Trevino, L., Jackson, L.A., and Dixon, R.A. (2011). Salicylic acid
689 mediates the reduced growth of lignin down-regulated plants. Proceedings of the National
690 Academy of Sciences 108, 20814-20819.
691 Gallego-Giraldo, L., Pose, S., Pattathil, S., Peralta, A.G., Hahn, M.G., Ayre, B.G., Sunuwar, J.,
692 Hernandez, J., Patel, M., Shah, J., Rao, X., Knox, J.P., and Dixon, R.A. (2018). Elicitors
693 and defense gene induction in plants with altered lignin compositions. The New phytologist
694 219, 1235-1251.
695 Gutierrez, L., Mongelard, G., Floková, K., Păcurar, D.I., Novák, O., Staswick, P., Kowalczyk, M.,
696 Păcurar, M., Demailly, H., and Geiss, G. (2012). Auxin controls Arabidopsis adventitious
697 root initiation by regulating jasmonic acid homeostasis. The Plant Cell 24, 2515-2527.

698 Hoffmann, L., Besseau, S., Geoffroy, P., Ritzenthaler, C., Meyer, D., Lapierre, C., Pollet, B., and
699 Legrand, M. (2004). Silencing of hydroxycinnamoyl-coenzyme A shikimate/quinate
700 hydroxycinnamoyltransferase affects phenylpropanoid biosynthesis. The Plant Cell 16,
701 1446-1465.
702 Kim, J., Dotson, B., Rey, C., Lindsey, J., Bleecker, A.B., Binder, B.M., and Patterson, S.E. (2013).
703 New clothes for the jasmonic acid receptor COI1: delayed abscission, meristem arrest and
704 apical dominance. PloS one 8, e60505.
705 Kleinboelting, N., Huep, G., Kloetgen, A., Viehoever, P., and Weisshaar, B. (2012). GABI-Kat
706 SimpleSearch: new features of the Arabidopsis thaliana T-DNA mutant database. Nucleic
707 acids research 40, D1211-1215.
708 Knoblauch, M., Knoblauch, J., Mullendore, D.L., Savage, J.A., Babst, B.A., Beecher, S.D.,
709 Dodgen, A.C., Jensen, K.H., and Holbrook, N.M. (2016). Testing the Münch hypothesis of
710 long distance phloem transport in plants. Elife 5, e15341.
711 Lakehal, A., and Bellini, C. (2019). Control of adventitious root formation: insights into synergistic
712 and antagonistic hormonal interactions. Physiologia plantarum 165, 90-100.
713 Lakehal, A., Dob, A., Rahneshan, Z., Novák, O., Escamez, S., Alallaq, S., Strnad, M., Tuominen,
714 H., and Bellini, C. (2020). ETHYLENE RESPONSE FACTOR 115 integrates jasmonate
715 and cytokinin signaling machineries to repress adventitious rooting in Arabidopsis.
716 bioRxiv, 2019.2012. 2027.886796.
717 Lakehal, A., Chaabouni, S., Cavel, E., Le Hir, R., Ranjan, A., Raneshan, Z., Novák, O., Păcurar,
718 D.I., Perrone, I., and Jobert, F. (2019). A Molecular Framework for the Control of
719 Adventitious Rooting by TIR1/AFB2-Aux/IAA-Dependent Auxin Signaling in
720 Arabidopsis. Molecular plant 12, 1499-1514.
721 Lee, S., Sundaram, S., Armitage, L., Evans, J.P., Hawkes, T., Kepinski, S., Ferro, N., and Napier,
722 R.M. (2014). Defining Binding Efficiency and Specificity of Auxins for SCFTIR1/AFB-
723 Aux/IAA Co-receptor Complex Formation. Acs Chem Biol 9, 673-682.
724 Li, X., Bonawitz, N.D., Weng, J.-K., and Chapple, C. (2010). The growth reduction associated with
725 repressed lignin biosynthesis in Arabidopsis thaliana is independent of flavonoids. The
726 plant cell 22, 1620-1632.

727 Melnyk, C.W., Schuster, C., Leyser, O., and Meyerowitz, E.M. (2015). A developmental
728 framework for graft formation and vascular reconnection in Arabidopsis thaliana. Current
729 Biology 25, 1306-1318.
730 Moreno-Risueno, M.A., Van Norman, J.M., Moreno, A., Zhang, J., Ahnert, S.E., and Benfey, P.N.
731 (2010). Oscillating gene expression determines competence for periodic Arabidopsis root
732 branching. Science 329, 1306-1311.
733 Morris, G.M., Huey, R., Lindstrom, W., Sanner, M.F., Belew, R.K., Goodsell, D.S., and Olson,
734 A.J. (2009). AutoDock4 and AutoDockTools4: Automated Docking with Selective
735 Receptor Flexibility. J Comput Chem 30, 2785-2791.
736 Munch, E. (1930). Stoffbewegungen in der Pflanze.
737 Muro-Villanueva, F., Mao, X., and Chapple, C. (2019). Linking phenylpropanoid metabolism,
738 lignin deposition, and plant growth inhibition. Current opinion in biotechnology 56, 202-
739 208.
740 Naseer, S., Lee, Y., Lapierre, C., Franke, R., Nawrath, C., and Geldner, N. (2012). Casparian strip
741 diffusion barrier in Arabidopsis is made of a lignin polymer without suberin. Proceedings
742 of the National Academy of Sciences 109, 10101-10106.
743 Noel, J.P., Austin, M.B., and Bomati, E.K. (2005). Structure–function relationships in plant
744 phenylpropanoid biosynthesis. Current Opinion in Plant Biology 8, 249-253.
745 Peer, W.A., and Murphy, A.S. (2007). Flavonoids and auxin transport: modulators or regulators?
746 Trends in plant science 12, 556-563.
747 Pettersen, E.F., Goddard, T.D., Huang, C.C., Couch, G.S., Greenblatt, D.M., Meng, E.C., and
748 Ferrin, T.E. (2004). UCSF chimera - A visualization system for exploratory research and
749 analysis. J Comput Chem 25, 1605-1612.
750 Ralph, J., Lapierre, C., and Boerjan, W. (2019). Lignin structure and its engineering. Current
751 opinion in biotechnology 56, 240-249.
752 Rasmussen, A., Hu, Y., Depaepe, T., Vandenbussche, F., Boyer, F.-D., Van Der Straeten, D., and
753 Geelen, D. (2017). Ethylene controls adventitious root initiation sites in Arabidopsis
754 hypocotyls independently of strigolactones. Journal of Plant Growth Regulation 36, 897-
755 911.
756 Saslowsky, D.E., Dana, C.D., and Winkel-Shirley, B. (2000). An allelic series for the chalcone
757 synthase locus in Arabidopsis. Gene 255, 127-138.

758 Schalk, M., Cabello-Hurtado, F., Pierrel, M.-A., Atanassova, R., Saindrenan, P., and Werck-
759 Reichhart, D. (1998). Piperonylic acid, a selective, mechanism-based inactivator of the
760 trans-cinnamate 4-hydroxylase: a new tool to control the flux of metabolites in the
761 phenylpropanoid pathway. Plant Physiology 118, 209-218.
762 Schilmiller, A.L., Stout, J., Weng, J.K., Humphreys, J., Ruegger, M.O., and Chapple, C. (2009).
763 Mutations in the cinnamate 4-hydroxylase gene impact metabolism, growth and
764 development in Arabidopsis. The Plant Journal 60, 771-782.
765 Schmid, N.B., Giehl, R.F., Döll, S., Mock, H.-P., Strehmel, N., Scheel, D., Kong, X., Hider, R.C.,
766 and von Wirén, N. (2014). Feruloyl-CoA 6′-Hydroxylase1-dependent coumarins mediate
767 iron acquisition from alkaline substrates in Arabidopsis. Plant Physiology 164, 160-172.
768 Steenackers, W., Klíma, P., Quareshy, M., Cesarino, I., Kumpf, R.P., Corneillie, S., Araújo, P.,
769 Viaene, T., Goeminne, G., and Nowack, M.K. (2017). cis-Cinnamic acid is a novel, natural
770 auxin efflux inhibitor that promotes lateral root formation. Plant physiology 173, 552-565.
771 Steenackers, W., El Houari, I., Baekelandt, A., Witvrouw, K., Dhondt, S., Leroux, O., Gonzalez,
772 N., Corneillie, S., Cesarino, I., and Inzé, D. (2019). cis-Cinnamic acid is a natural plant
773 growth-promoting compound. Journal of experimental botany 70, 6293-6304.
774 Steffens, B., and Rasmussen, A. (2016). The physiology of adventitious roots. Plant Physiology
775 170, 603-617.
776 Tan, S., Abas, M., Verstraeten, I., Glanc, M., Molnár, G., Hajný, J., Lasák, P., Petřík, I., Russinova,
777 E., and Petrášek, J. (2020). Salicylic acid targets protein phosphatase 2A to attenuate growth
778 in plants. Current Biology 30, 381-395. e388.
779 Trott, O., and Olson, A.J. (2010). Software News and Update AutoDock Vina: Improving the
780 Speed and Accuracy of Docking with a New Scoring Function, Efficient Optimization, and
781 Multithreading. J Comput Chem 31, 455-461.
782 Van de Wouwer, D., Vanholme, R., Decou, R., Goeminne, G., Audenaert, D., Nguyen, L., Höfer,
783 R., Pesquet, E., Vanholme, B., and Boerjan, W. (2016). Chemical genetics uncovers novel
784 inhibitors of lignification, including p-iodobenzoic acid targeting CINNAMATE-4-
785 HYDROXYLASE. Plant physiology 172, 198-220.
786 Vanholme, B., El Houari, I., and Boerjan, W. (2019a). Bioactivity: phenylpropanoids' best kept
787 secret. Current opinion in biotechnology 56, 156-162.

788 Vanholme, B., Desmet, T., Ronsse, F., Rabaey, K., Van Breusegem, F., De Mey, M., Soetaert, W.,
789 and Boerjan, W. (2013). Towards a carbon-negative sustainable bio-based economy.
790 Frontiers in plant science 4, 174.
791 Vanholme, R., De Meester, B., Ralph, J., and Boerjan, W. (2019b). Lignin biosynthesis and its
792 integration into metabolism. Current opinion in biotechnology 56, 230-239.
793 Vanholme, R., Sundin, L., Seetso, K.C., Kim, H., Liu, X., Li, J., De Meester, B., Hoengenaert, L.,
794 Goeminne, G., and Morreel, K. (2019c). COSY catalyses trans–cis isomerization and
795 lactonization in the biosynthesis of coumarins. Nature plants 5, 1066-1075.
796 Veldstra, H. (1953). The relation of chemical structure to bio-logical activity in growth substances.
797 Annual Review of Plant Physiology 4, 151-198.
798 Verstraeten, I., Schotte, S., and Geelen, D. (2014). Hypocotyl adventitious root organogenesis
799 differs from lateral root development. Frontiers in plant science 5, 495.
800 Vogt, T. (2010). Phenylpropanoid biosynthesis. Molecular plant 3, 2-20.
801 Wong, W.S., Guo, D., Wang, X.L., Yin, Z.Q., Xia, B., and Li, N. (2005). Study of cis-cinnamic
802 acid in Arabidopsis thaliana. Plant Physiology and Biochemistry 43, 929-937.
803 Xuan, W., Audenaert, D., Parizot, B., Möller, B.K., Njo, M.F., De Rybel, B., De Rop, G., Van
804 Isterdael, G., Mähönen, A.P., and Vanneste, S. (2015). Root cap-derived auxin pre-patterns
805 the longitudinal axis of the Arabidopsis root. Current Biology 25, 1381-1388.
806 Zhao, X., Wang, J., Yuan, J., Wang, X.L., Zhao, Q.P., Kong, P.T., and Zhang, X. (2015). NITRIC
807 OXIDE-ASSOCIATED PROTEIN1 (AtNOA1) is essential for salicylic acid-induced root
808 waving in Arabidopsis thaliana. The New phytologist 207, 211-224.
809 Zipfel, C., Robatzek, S., Navarro, L., Oakeley, E.J., Jones, J.D., Felix, G., and Boller, T. (2004).
810 Bacterial disease resistance in Arabidopsis through flagellin perception. Nature 428, 764-
811 767.

812
813

FIGURE & TABLE LEGENDS

Figure 1. Inhibition of C4H results in strong seedling phenotypes.

(a) The first two steps of the general phenylpropanoid pathway, with the conversion of phenylalanine to cinnamic acid by PAL and subsequent conversion to *p*-coumaric acid by C4H. Alternatively, *trans*-cinnamic acid can isomerize to its *cis*-isomer under influence of UV. The known C4H-inhibitor PA is indicated on the figure in red. PAL = PHENYLALANINE AMMONIA LYASE; C4H = CINNAMATE-4-HYDROXYLASE; PA = piperonylic acid. (b) Phenotype of 4-weeks-old Col-0 WT, heterozygous *c4h*-mutant and homozygous *c4h*-mutant. An inset is made focusing on the homozygous *c4h*-mutant (scale bar: 0.1 cm). (c-d) Average primary root length (c) and LRD (d) of WT and *c4h-4* seedlings (n>20). (e). Average number of ARs of WT and *c4h-4* etiolated seedlings (n>50). (f) Phenotype of etiolated WT and *c4h-4* seedlings grown on ½ MS medium (scale bar: 0.5 cm). ARs located at the top third are indicated with a yellow arrow, ARs located at the bottom two thirds are indicated with a blue arrow. (g-h) PA dose-response curves for primary root length (g) and LRD (h) (n>20). (i) PA dose-response graph for average number of ARs of etiolated seedlings (n>40). (j) Phenotype of etiolated seedlings grown on ½ MS medium supplemented with or without 50 µM PA (scale bar: 1 cm). ARs located at the top third are indicated with a yellow arrow, ARs located at the bottom two thirds are indicated with a blue arrow. An inset was made focusing on the adventitious roots formed upon PA treatment (scale bar: 0.1 cm). Yellow coloration represents the top third of the hypocotyl; blue coloration represents the lower two-thirds. Error bars represent 95% confidence intervals. Asterisks indicate significant differences compared to the corresponding mock-treatment (*P < 0.01, **P < 0.001, ***P <0.0001; c: Student's t-test; d,e,h,i: GEE model; g: ANOVA, Dunnett's test).

Figure 2. PA-treatment serves as an adequate substitute for the *c4h-4* mutant.

Principal component analysis score plots for the metabolic profiles obtained by LC-MS of etiolated Col-0 WT, *c4h-4* and 50 µM PA-treated WT seedlings (n>7). Each datapoint represents 8 biological replicates.

Figure 3. Inhibition of C4H results in auxin transport inhibition.

(a) Average number of ARs of etiolated Col-0 WT, the jasmonate signaling mutant *coi1-21*, the ethylene signaling mutant *etr1-3* and the auxin signaling mutant *tir1afb2afb3* grown on ½ MS medium supplemented with (+) or without (-) 50 µM PA (n>20). Yellow coloration represents the top third of the hypocotyl; blue coloration represents the lower two-thirds. (b) Kymographs of *pDR5::LUC* intensity along the hypocotyl of etiolated seedlings during a 12h period. Seedlings were etiolated and grown on plates with/without 50 µM PA (n>50). (c) Graph showing normalized intensity of the *pDR5::LUC* signal over the hypocotyl of etiolated Arabidopsis seedlings grown on plates with or without 50 µM PA (n>50). SAM: shoot apical meristem. (d) Chemical structures of IAA and PA. (e) Docking results in the best possible pose for IAA and PA in the lower region of the TIR1 pocket. The bottom shows the superimposed structures of PA and IAA from two perspectives (f) Surface Plasmon Resonance analysis of auxin-dependent interaction of TIR1 and AFB5 with IAA DII. Each sensorgram shows the binding with 50 µM IAA (blue), an auxin-free injection (red) and the data for 50 µM PA (green). Lower panels show the sensorgrams from the anti-auxin assay with 5 µM IAA (blue dashed line) or 5 µM IAA plus 50 µM PA (green). (g) Auxin transport capacity of mock, PA and NPA-treated seedlings (n=9). DPM: disintegrations per minute. Error bars represent 95% confidence intervals. Asterisks indicate significant differences compared to the corresponding mock-treatment (*P < 0.01, **P < 0.001, ***P <0.0001; a: GEE model, g: ANOVA, Dunnett's test).

Figure 4. Auxin transport inhibition upon blocking C4H is caused by both an accumulation of *c*-CA and a depletion in monolignols.

(a-b) Profiling of *t*-CA (a) and *c*-CA (b) levels of etiolated seedlings grown on ½ MS medium supplemented with or without 50 µM PA and UV (n=5). Values on the y-axis indicate the absolute amount of *t*-CA (a) or *c*-CA (b) per mg of dry weight (DW). (c) Auxin

transport capacity of etiolated seedlings treated with or without 50 µM PA and UV (n=9). (d-j) Average number of ARs of etiolated (d) Col-0 grown on ½ MS medium supplemented with or without 50 µM PA and UV (n>60). (e) Col-0 and *NahG-OE*, deficient in salicylic acid, supplemented with or without 50 µM PA (n>100). (f,g) Col-0 grown on ½ MS medium supplemented with 50 µM PA and either 200 µM *p*CA (f) or 100 µM quercetin (g) (n>40). (h) Col-0 and the flavonoid mutant *tt4* (n>100). (i) Col-0 grown on ½ MS medium supplemented with or without 50 µM PA and 100 µM ConAld (n>50). (j) Col-0 grown on ½ MS medium supplemented with or without 50 µM PA, 100 µM ConAld and UV (n>50). Yellow coloration represents the top third of the hypocotyl; blue coloration represents the lower two-thirds. Error bars represent 95% confidence intervals. Letters a-d are given to distinguish statistically significant results ($p<0.01$; a-c: ANOVA, Tukey test; d-j: GEE model).

Figure 5. Inhibition of C4H perturbs long-distance auxin transport through the phloem due to a depletion in lignin.

(a) Graph showing normalized intensity of the *pDR5::LUC* signal of etiolated Arabidopsis seedlings grown on plates with or without 50 µM PA and 100 µM ConAld (n>30). These were then transferred to ½ MS medium and treated for 1h with luciferin, upon which the signal intensity was measured and normalized for the length of the hypocotyl. (b) Wiesner staining of etiolated seedlings grown on ½ MS medium supplemented with or without 50 µM PA and 100 µM ConAld. For each treatment, the entire hypocotyl is shown on the left (scale bar: 1 mm) and a magnification on the right (scale bar: 10µm). (c) Transverse sections stained with toluidine blue and counterstained with ruthenium red of etiolated seedlings grown on ½ MS medium supplemented with or without 50 µM PA and 100 µM ConAld. Pictures are representative for > 25 hypocotyls (scale bar: 10 µm). (d) Xylem transport assays using the fluorescent probe CFDA. Etiolated seedlings were grown on ½ MS medium supplemented with or without 50 µM PA and 100 µM ConAld and the hypocotyl was excised directly above the hypocotyl-root junction. CFDA was administered to the bottom of the hypocotyl and fluorescence was assessed over time in the SAM (n>100). SAM: shoot apical meristem. (e) Phloem transport assays using the fluorescent probe CFDA. Etiolated seedlings were grown on ½ MS medium supplemented with or

without 50 µM PA and 100 µM ConAld before CFDA was administered to the cotyledons. Fluorescence was then assessed over time in the hypocotyl-root junction (n>100).

Figure 6. Confirmation of results in the *c4h-4* mutant

(a) Average number of ARs of etiolated Col-0 WT and *c4h-4* seedlings grown on ½ MS medium supplemented with or without 100 µM ConAld (n>50). Yellow coloration represents the top third of the hypocotyl; blue coloration represents the lower two-thirds. Error bars represent 95% confidence intervals. Letters a-d are given to distinguish statistically significant results for top third and a'-d' for bottom two thirds ($p<0.01$; GEE model). (b) Xylem transport assays using the fluorescent probe CFDA. Etiolated Col-0 WT and *c4h-4* seedlings were grown on ½ MS medium supplemented with or without 100 µM ConAld and the hypocotyl was excised directly above the hypocotyl-root junction. CFDA was administered to the bottom of the hypocotyl and fluorescence was assessed over time in the SAM (n>20). SAM: shoot apical meristem. (c) Phloem transport assays using the fluorescent probe CFDA. Etiolated Col-0 WT and *c4h-4* seedlings were grown on ½ MS medium supplemented with or without 100 µM ConAld before CFDA was administered to the cotyledons. Fluorescence was then assessed over time in the hypocotyl-root junction (n>30).

Figure 7. Model explaining the phenotypic effects upon inhibition of C4H

Graphical model displaying the physiological effects upon blocking C4H in the hypocotyl. (a) Given a functional phenylpropanoid pathway, baseline levels of *c*-CA are produced and normal lignin deposition takes place. Functional polar auxin transport and phloem transport result in normal auxin distribution pattern. (b) Upon blocking C4H, *c*-CA levels are elevated due to increased UV-mediated conversion from t-CA, which would lead to a reduced cell-to-cell auxin transport. In addition, lignin deposition is reduced, leading to a perturbed long-distance auxin transport through the phloem. As a consequence, auxin distribution is affected, resulting in an apical accumulation of auxin. Dashed line from phenylalanine to *c*-CA represents a putative biosynthetic route towards *c*-CA. PAL =

928 PHENYLALANINE AMMONIA LYASE; C4H = CINNAMATE-4-HYDROXYLASE; *t*-CA =
929 *trans*-cinnamic acid; *c*-CA = *cis*-cinnamic acid; *p*CA = *para*-coumaric acid.
930
931 **Table 1. Inhibition of C4H perturbs the PPP.**

932 List of compounds that were characterized upon LC-MS profiling of etiolated Col-0 WT,
933 *c4h-4* and Col-0 seedlings treated with 50 µM PA (n>7). Each data point represents 8
934 biological replicates. For each metabolite, a unique number (No.), mass-to-charge ratio
935 (*m/z*), retention time (RT), peak area ± SD and fold-change compared to the WT are given.
936